Master's thesis

Surface engineering for injection control and hysteresis reduction in Perovskite Solar Cells

Author: Marta Vallés Pelarda
Supervisor: Dr. Iván Mora Seró
Master's Degree in Applied Physics
Universitat Jaume I
Castellón, July 2016

Content

Acknowledgements

First of all, I would like to express my gratitude to Dr. Iván Mora, my supervisor, for his help, dedication to this work and time spent in my learning. He guided me during the development of the work. I would also like to thank Prof. Juan Bisquert, director of the Institute of Advanced Materials (INAM) for providing me the opportunity to do my master thesis in the institute, in the Group of Photovoltaic and Optoelectronic Devices. In addition, thanks to SEFIN for the financial support for the master degree.

I would like to thank Bruno Clasen and Rafael Sánchez for their help in this work and the rest of the group, especially to Drialys Cardenas, Nuria Vicente and Lucía Navarro for their unconditional support.

I would like to thank to *Serveis Centrals* at UJI, where the structural characterization was performed.

Finally, I cannot forget to thank Ines García, Agustín Molina, and Nazario Martín, from Complutense University of Madrid and Madrid Institute of Advanced Studies (IMDEA Institute), for synthesizing the fullerene derivatives employed in this work.

List of abbreviations

CB	Conduction Band
CCD	Charge-Coupled Device
CL	Compact Layer
DMF	Dimethylformamide
DSSC	Dye-Sensitized Solar Cell
EL	Electroluminescence
EQE	External Quantum Efficiency
ESC	Electron Selective Contact
FF	Fill Factor
FTO	Fluorine-doped Tin Oxide
HI	Hysteretic Index
HOMO	Highest Occupied Molecular Orbital
HTM	Hole Transporting Material
HSC	Hole Selective Contact
J_{mp}	Current density at maximum power
J_{sc}	Short Circuit Current Density
LED	Light-Emitting Diode
LUMO	Lowest Unoccupied Molecular Orbital
NS	Nanostructured
OPV	Organic Photovoltaics
PL	Photoluminescence
P_{mp}	Maximum Power
PSC	Perovskite Solar Cell
PV	Photovoltaics
QDSC	Quantum Dot Solar Cell
SAM	Self-Assembled Monolayer
SC	Solar Cell
SEM	Scanning Electron Microscopy
TBP	4-tert-butylpyridine
TCO	Transparent Conductive Oxide
V_{mp}	Voltage at maximum power
V_{oc}	Open Circuit Potential
VB	Valence Band

Abstract

Hybrid halide perovskites, such as $CH_3NH_3PbI_3$ are among the most promising absorbers materials in photovoltaics due to its direct band gap, high absorption coefficient and low charge recombination.[1,2] In addition, they have the benefits of being prepared by low temperature solution processes which are low cost.[3,4] However, the interfaces between the perovskite and the selective contacts are still decisive for obtaining a better performance of the device. In addition, interfaces also play a critical role on the hysteresis present in the J-V curves that has been detected in Perovskite Solar Cells (PSCs), indicating that the current is dependent on the direction and speed of the scanning.[5,6]

Modifying the electron selective contact with a self-assembled monolayer (SAM) of fullerene derivatives has shown to enhance the photocurrent and to have a positive effect on the hysteresis, as reported for example by Wojciechowski et al.[7] This fullerene derivative contains a functional group to anchor, by chemisorption, onto the selective contact surface, modifying the interface and improving the electron extraction.[8]

This work is focused on the use of some fullerene derivatives containing different functional groups to anchor onto the scaffold and the compact layer of TiO_2. In addition, the effect of removing the compact layer has been studied in combination with the use of fullerenes.

Chapter 1. Introduction

The increasing demand of energy, the finite reserves of the traditional energy sources and their deleterious implications as global warming have caused that the interest on renewable energies is progressively a more relevant issue that galvanizes enormous efforts from the research community. Fossil fuels are the most common energy sources for providing power to our society. However, these types of energy are non-renewable and have finite reserves. Among the renewable energies that are being studied, solar energy awakened interest as it is the one with the highest potentiality as the Earth receives from the Sun, in just one hour, all the energy used by the humankind in one year.[4,9-11]

There are two main forms of leverage solar energy. One of them is thermal conversion, which consists in obtaining work from the thermal energy. For example, this solar energy conversion is used as water heater. The other one is photovoltaic conversion, which consists in obtaining excited electrons due to the absorption of photons, which can generate an electric current. The generation of electric current directly from the sunlight has many advantages, for example, it does not generate any waste like other energy sources (coal, nuclear energy…), and it is ready to be used, stored or transported. For that purpose, devices known as solar cells (SCs) are employed for photovoltaic conversion.[10,12]

1.1. Solar cells and their characteristic parameters

Solar cells are composed by different layers with specific purposes. The first important layer is formed by a light absorbing material, necessary to achieve the energy conversion. The absorber can be a single molecule, an organic polymer or a semiconductor, which is conventionally defined as a dielectric with a relatively small band gap between the valence band (VB) and conduction band (CB) from 0.5 to 3eV approximately.

Figure 1.1 shows a scheme of the main processes involved inside the SC. When this material is illuminated, the incident photons whose energy is equal or higher than the band gap of the material excite the electrons from the VB to the CB forming an electron-hole pair. In the case of a molecule or an organic polymer, the electronic transition occurs between the HOMO (Highest Occupied Molecular Orbital) and LUMO (Lowest Unoccupied Molecular Orbital) of the molecule. In order to transform the free energy acquired by the absorbing material due to photon absorption into external work, a second step is needed to complete the photovoltaic process: the charge separation at the selective contacts, electron selective contact (ESC) and hole selective contact (HSC).[10,13,14] In addition, SC performance will be optimized if recombination process between electrons and holes, dashed line in Figure 1.1, is minimized.

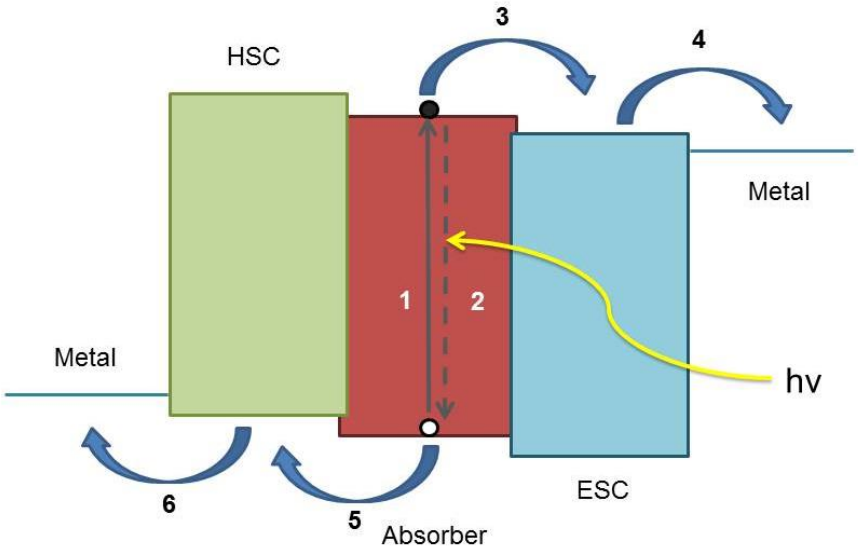

Figure 1.1 Energy diagram showing the main processes that occur in a SC: (1) light absorption, (2) recombination, (3) electron transport to the ESC (4) electron transport along the ESC and extraction by the metal contact, (5) hole transport to the HSC and (6) hole transport along the HSC and extraction by the metal contact.

The characteristic parameters of the solar cells are the photocurrent, open circuit potential, fill factor and efficiency.

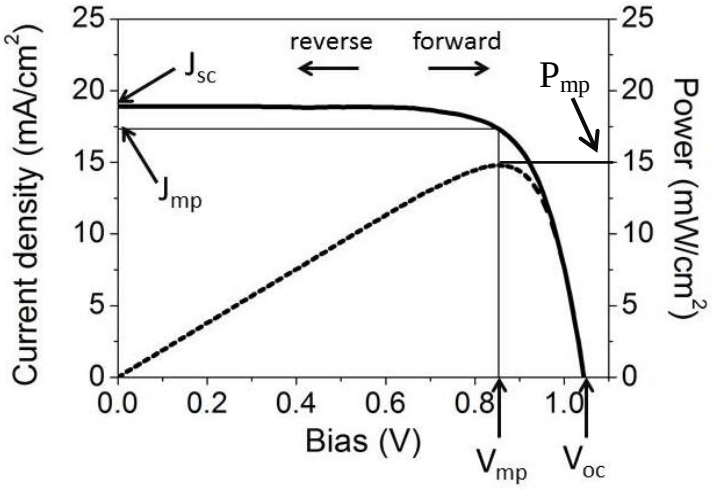

Figure 1.2 Current-voltage curve (solid line) showing some representative parameters and power obtained from the solar cell (dashed line).

The photocurrent density, also known as short circuit current density (J_{sc}), is the current per unit area obtained at short circuit under illumination. Photocurrent is affected by the absorption properties of the absorber but also by the charge collection efficiency.

The open circuit potential (V_{oc}) is defined by the difference in chemical potential of the electrons and the holes at the extracting contacts, known as Fermi level splitting in semiconductors. This difference in electrochemical potential is free energy that can be transformed in useful power by charge separation at the selective contacts. Note that effective V_{oc} will be lower than the Fermi level splitting due to recombination.

The fill factor (FF) is associated with the form of the J-V curve. It is defined as:

$$FF(\%) = \frac{J_{mp} \cdot V_{mp}}{J_{sc} \cdot V_{oc}} \cdot 100 \qquad \textbf{(1)}$$

Where J_{mp} and V_{mp} are the current and voltage at the maximum power point, respectively, see Figure 1.2. The efficiency which is the percentage of the incident power that is transformed into electrical power is defined as:

$$Eff(\%) = \frac{P_{mp}}{P_{in}} \cdot 100 \qquad \textbf{(2)}$$

Where P_{in} is the input power (100mW/cm^2 at 1sun) and P_{mp} is the maximum power point of the solar cell. One interesting phenomenon observed in the J-V curves of perovskite solar cells and whose origin is not fully understood is the hysteresis, see Figure 1.3. Depending on the scan rate and direction, the device has a different behavior and consequently, the solar cell efficiency, calculated from J-V curve, depends on them. It is called reverse scan when the direction of the applied bias is from high voltage to zero bias and forward direction when the applied bias goes from zero to high bias.[5,14,15]

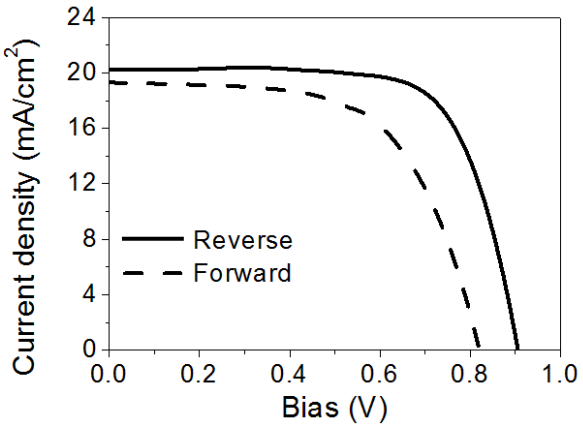

Figure 1.3 J-V curve showing the effect of the hysteresis

1.2. History of the solar cells

Over the last 50 years, several kinds of solar cells have been developed and are under exhaustive research to improve their efficiency such as thin film SCs (CdTe, CIGS), SCs with GaAs as absorber and crystalline silicon SCs (single crystal, multicrystalline, silicon heterostructures and thin-film crystal).[16,17] The most commercialized is the silicon solar cell, first developed in 1954 with 6% of efficiency[18] using a single-crystal cell. Si solar cell is formed by a p-n homojunction, meaning that has an n-type part (the majority carriers are the electrons) and a p-type part (the majority carriers are the holes) inside the same material, and the metal contacts. The electrons are excited to the conduction band and go from the p-type region to the n-type region, and the holes in the valence band go from the n-type to the p-type region. Thus, p-n juction acts as selective contact.

However, silicon is not one of the ideal materials for PV because, among other reasons, it is an indirect band gap semiconductor, which means that the maximum of the VB and the minimum of the CB have not the same momentum *k* and so a lower probability of absorbing light.[11,17,19] Consequently, thicker devices are needed in order to absorb all the incident light. In addition, high temperature is needed for their fabrication. For those reasons, in the last few years, some emerging PV technologies have taken more importance, such as Dyed-Sensitized Solar Cells (DSSCs), Organic Cells (OPV), Quantum Dot Solar Cells (QDSCs) and Perovskite Solar Cells (PSCs).

In the 1980s, the first solar cells based on the use of polymers were developed.[20] However, in 1986, Tang[21] developed solar cells with a donor and an acceptor organic molecules, increasing their efficiency to 1%. Several types of heterojunctions have been investigated, being the most studied polymer/fullerene blends due to the electron affinity of fullerenes. In this type of SCs, the donor molecule is photoexcited and as the LUMO of the acceptor is less energetic than the donor LUMO, the electron is relaxed to the acceptor LUMO and then to the metal contact.[21]

In the beginning of the 1990s, DSSCs were developed. The absorber is a dye molecule that sensitizes the surface of mesoporous TiO_2, which is on the top of a plastic or a glass coated with a transparent conducting oxide (TCO), like fluorine-doped tin oxide (FTO). After the excitation of an electron by light from the HOMO to the LUMO of the dye molecule, the electron is injected into the TiO_2 and the molecule is left on its oxidized state. It is reduced by the presence of an electrolyte, usually iodide/ triiodide (I^-/I^{3-}) redox system in an organic solvent. I^{3-} ions diffuse through the solvent to the cathode coated with a platinum catalyst which regenerates the iodide ions.[22] Later, QDs replaced the dyes as absorbers in DSSCs. The light excites the electrons in the QD producing an electron-hole pair; the electron is transferred to the TiO_2 and the hole is transferred to the HTM or an electrolyte.[23]

Between 2006 and 2008, T. Miyasaka and co-workers employed perovskites ($CH_3NH_3PbI_3$ and $CH_3NH_3PbBr_3$) as absorbers with I^-/I^{3-} redox couple or a solid state hole conductor (polypyrrole carbon black composite). In 2009, they reported a sensitized solar cell with $CH_3NH_3PbI_3$ employing I^-/I^{3-} redox couple with 3.8% efficiency.[24] After that, an exhaustive research in the field of perovskites has been performed, obtaining solar cells with 22.1% efficiency in 2016 by Korea Research Institute of Chemical Technology (KRICT) and Ulsan National Institute of Science and Technology (UNIST) in 2016. PSCs are considered one of the most promising technologies as in less than 10 years, they have increased from 3.8% to 22.1%.[25]

1.3. Perovskite Solar Cells

The perovskite is a type of crystalline structure with the general formula ABX_3. There are a huge amount of compounds that have this structure, however, in the most common materials employed as absorber in SCs, A is an organic cation ($CH_3NH_3^+$, $CH_3CH_2NH_3^+$…), B is a metallic cation generally lead (Pb^{+2}) or tin (Sn^{+2}) and X is an halide (I^-, Br^-, Cl^-). In Figure 1.4, the perovskite structure with the formula $CH_3NH_3PbI_3$ is shown. A methylammonium molecule occupies the centre, iodide atoms occupy the vertices of the octahedra and lead atoms occupy their centres.[25,26] Although the band gap of the $CH_3NH_3PbI_3$ perovskite is 1.52eV, the band gap and the optical absorption of this perovskite can be modified to cover the major part of the visible spectrum by incorporating two halides, for example iodide with bromide or bromide with chloride.[2] Nevertheless, $CH_3NH_3PbI_3$ perovskite formed using lead chloride precursor does not show a change in the band gap, attributed to the difficulty of incorporating chloride to the PbI_6 octahedron.[1,2]

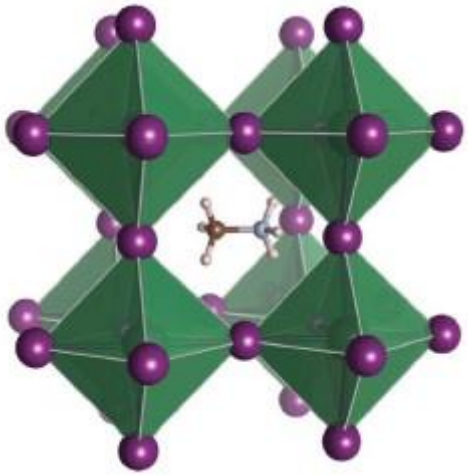

Figure 1.4 $CH_3NH_3PbI_3$structure.[26]

Common PSCs devices are prepared using FTO as TCO with a compact layer of an electron selective material like TiO_2. A mesoporous layer of semiconductor materials (TiO_2 or ZnO) or an insulator (Al_2O_3 or ZrO_2) on the top of the compact layer is extensively used, as helps to obtain high efficiency, and the perovskite is infiltrated within this layer. A hole selective material (HSM) is employed between the perovskite and the metal contact (Au or Ag). The most common HSM is 2,2',7,7'-tetrakis-(N,N'-dimethoxyphenyl-amine)-9,9'-spirobifuorene (spiro-OMeTAD) with some additives to improve the conductivity.[27] It is really important to have good selective contacts to extract the electrons and holes before the recombination takes place. The recombination is a phenomenon that has a strong influence in the efficiency. The rate of charge extraction should be higher than the recombination, otherwise these losses affect to the open circuit potential.

1.4. Fullerenes modifying the electron selective contact

As mention before, the selective contacts should be capable of separating correctly the charges to avoid recombination. TiO_2 was supposed to be one of the best electron extraction and transport materials because of its chemical stability, easy preparation, closeness of CB with hybrid perovskites and the depth of its VB, which blocks the hole conduction. Nevertheless, TiO_2 has oxygen vacancies specially at the surface which act as trap levels[28] and therefore, the interface between the perovskite and the TiO_2 is still an important issue to be optimized. Modifying the interface the electron injection and electron transfer can be significantly enhanced, as well as reducing the charge recombination. An alternative that has been investigated is the functionalization of this layer with fullerene derivatives. Fullerenes have high electron affinity and are good electron acceptors. Their π-conjugated structure enables the charge dislocation, enhancing the electron extraction. In addition, they have reduced the hysteretic effect present in PSCs. To functionalize the TiO_2 surface, the fullerene should have a functional group to enable the anchor by chemisorption, it is usually a carboxyl group (-COOH). Figure 1.5 shows the anchor of a fullerene derivative to the TiO_2.[7,8,29,30]

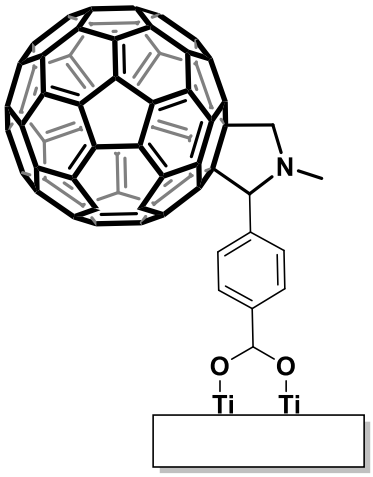

Figure 1.5 Fullerene derivative (AM87) showing the anchor onto the TiO_2 surface.

Other alternative use of the fullerene derivatives is depositing a layer onto the FTO instead of a monolayer of these fullerenes, acting as ESC replacing the TiO_2. It has been reported that it can successfully replace the n-type contact and being stable.[6]

1.5. Aim of the work

Taking into account this brief introduction, the main objective of this work is to study two important issues for perovskite solar cells. The first one is the hysteresis, which affects directly the efficiency of the devices, and how this hysteresis is affected by the use of a fullerene SAM layer or the use of a compact TiO_2 ESC. The other one is the interface between the electron selective contact and the perovskite, which should be modified to enhance the electron injection. For that purpose, the functionalization of the TiO_2 with a SAM of different fullerene derivatives has been analyzed. The effect of these fullerene derivatives was evaluated in order to check the importance of the anchoring group structure and the opposite part, which is in contact with the perovskite. The characteristic parameters of these devices, including the hysteresis, are studied, as well as the photoluminescence and electroluminescence. Furthermore, the morphology of the different layers is characterized. In addition, other objective of this work is to study the effect of the fullerenes without the compact layer, so that in future works, this layer could be replaced by SAM fullerenes. The same characterization has been carried out with these devices.

Chapter 2. Experimental section

2.1. Deposition techniques

2.1.1. Spray pyrolysis

This method is a chemical deposition process employing a solution precursor. It consists in the generation of an aerosol of the precursor solution which is sprayed onto the heated surface of the substrate. The sprayed solution is thermally decomposed on the hot substrate surface, producing the formation of the desired material, in our case a layer of metal oxide used as electron selective contact.[31] The most influential parameters on the final structure and properties of the deposited films are the temperature and the precursor solution.

The equipment used consists of an atomizer, a heater and a temperature controller, as shown in Figure 2.1. In this case, the atomizer is an air blast using oxygen as propellant gas that also helps in the oxidation when the material to be deposited is an oxide.

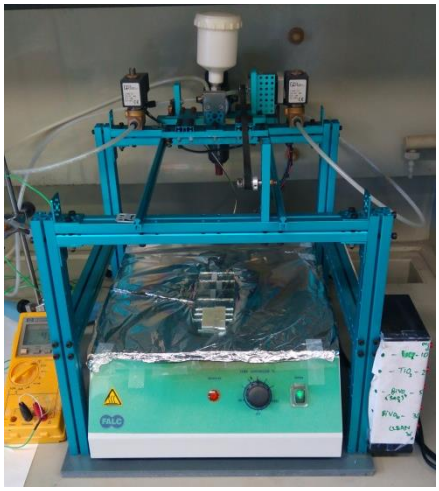

Figure 2.1 Spray pyrolysis equipment.

2.1.2. Spin Coating

Spin Coating is a physical deposition process employing a solution. It consists in the application of a solution to a substrate before or while the substrate is spinning at a chosen speed. A uniform thin film remains on the substrate as most of the solution is ejected as a result of the angular velocity. This technique allows the formation of homogeneous and highly reproducible films. The solvent and the concentration of the precursors are essential parameters for the thickness, morphology and surface topography of the film. The rotational speed, viscosity, volatility, diffusivity and molecular weight have also a strong influence on them. The volume of solution, the rate of deposition and the spinning time have a lower influence.[32]

Figure 2.2 Spin-coater.

2.1.3. Dip coating

Dip coating is a chemical deposition method employing a solution. In this technique, the substrate is immersed a controlled time in a solution which contains the material that is going to be deposited. When the substrate is removed from the solution, the solvent is evaporated, and the material no adsorbed is removed by rinsing.

2.1.4. Thermal evaporation

This method consists in the evaporation of a material by heating it at high vacuum. When the vapour pressure of the material is significant, atoms or molecules from the surface are detached.[33]

2.2. Characterization techniques

2.2.1. Current-Voltage curves

This characterization technique consists in applying a voltage sweep to the device and observing the relationship of the applied bias and the resulting current. The current-voltage curves were measured under illumination in order to determine solar cell performance, using an Abet Technologies Sun 2000 Class A solar simulator. The filter used was AM1.5G, the radiation was 1 sun (1000W m^{-2}) and the scan rate was 50mV/s. The measures were performed using a mask so that the illuminated area is 0.087cm^2. The J-V curves were measured in both scan directions: forward and reverse scan.

2.2.2. Photoluminescence (PL)

The PL is the light emission by radiative recombination of photoexcited carriers after light absorption. For the PL measurements, a commercial red laser diode (650nm, 319mW/cm^2) was used as excitation source. To avoid the presence of the excitation light peak in the spectra, a FGL400S glass filter was employed. The measurements were carried out using a spectrophotometer CCD detector (charge-coupled device, AndoriDUS DV 420A-OE) coupled with a spectrograph as a diffraction grating (Newport 77400).

2.2.3. Electroluminescence (EL)

The EL is the light emission by radiative recombination when applying a voltage. EL measurements were carried out using the equipment described for the PL measurements but coupled with a potentiostat (Gamry Reference 3000). The potentiostat is used to apply a DC bias to the devices. The EL measurements were carried out at different voltages and were performed in dark conditions at room temperature and under nitrogen flow to avoid sample degradation.

From the different EL spectra and chronoamperometries, the emission External Quantum Efficiency (EQE) was calculated. A calibration is needed to obtain the incident photons, it was carried out using a commercial GaAs infrared LED (EL-23G model, λ_{max}=940nm, 28.3Wsr^{-1}m^{-2}).

2.2.4. Scanning Electron Microscopy (SEM)

The Scanning Electron Microscope was a JEOL 7001F. It is equipped with an energy dispersive spectroscopy system INCA 350 (Oxford) and a wavelength dispersive system INCA Wave 200 (Oxford). The parameters used were acceleration voltage 15kV and working distance 10nm.

2.3. Device preparation

Two different structures of the devices were employed, as shown in Figure 2.3a and Figure 2.3b. Complete devices were prepared: on top of the FTO coated glass substrates, a compact layer of TiO_2 was deposited, then a scaffold of mesoporous TiO_2, a layer of perovskite which composition is $CH_3NH_3PbI_3$, a layer of spiro-OMeTAD and a layer of gold. See below for more details. Moreover, devices without the compact layer of TiO_2 were also prepared.

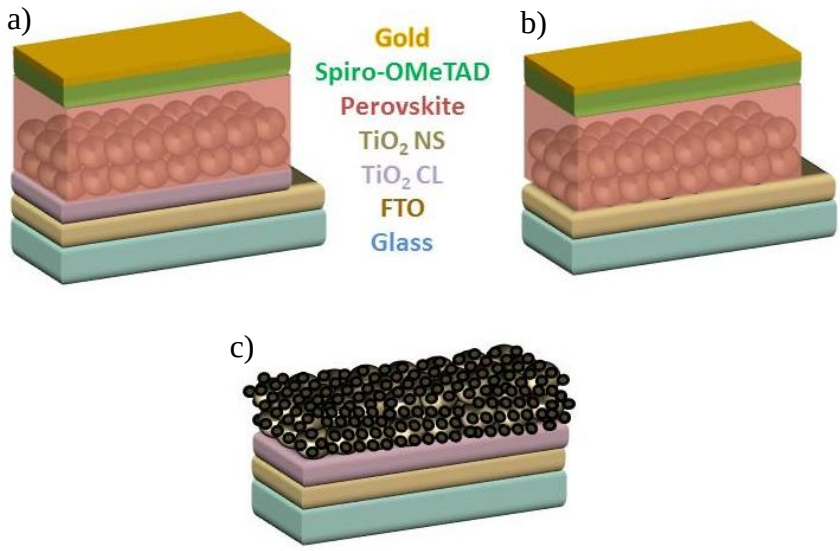

Figure 2.3 (a), (b) Solar cell structures showing the different layers, structure b has no compact TiO_2.**(c)** Solar cell structure showing the modification of the TiO_2 surface by the fullerene derivatives.

In Figure 2.3c, the modification of the surface of the TiO_2 scaffold and the compact layer by the SAM of the fullerene derivatives is also illustrated. The fullerene derivatives employed, shown in Figure 2.4, contain a functional group which enables the anchor by chemisorption onto the TiO_2 surface.

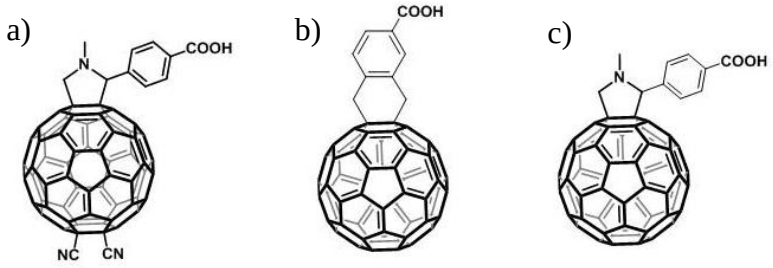

Figure 2.4 Structural formula of the different fullerene derivatives **(a)** IG321, **(b)** AM87 and **(c)** AM90.

Different chemicals have been used in the realization of this work. Titanium diisopropoxidebis(acetylacetonate), lead chloride, dimethylformamide (DMF), anhydrous chlorobenzene, lithium bis(trifluoromethylsulphonyl)imide (Li-TFSI) and 4-tert-butylpyridine (TBP) were purchased from Sigma-Aldrich. TiO_2 18NRT paste was purchased from Dyesol and methylammonium iodide (MAI) was purchased from TCI. All the materials were used as received. The different fullerene derivatives were synthesized at IMDEA Institute as detailed in the annex.

The devices were made using FTO coated glass substrates (2.49x2.49cm^2). Approximately 8mm of FTO were chemically etched with zinc powder and HCl 2M. The substrates were washed with distilled water and cleaned with a solution of milliQ water and soap Extran® MA neutral. After that, they were sonicated for 15 minutes in a new solution of milliQ water and soap, rinsed with milliQ water and sonicated for 15 minutes in a solution of ethanol. Finally, they were rinsed with acetone and dried with compressed air.

Before depositing the TiO_2 compact layer (CL), a UV/ozone treatment was performed for 15 minutes to remove the residual organic matter or any contaminant present in the FTO surface. TiO_2 compact layer was deposited onto the substrates by spray pyrolysis at 450ºC with oxygen as carrier gas. The precursor solution was prepared with titanium diisopropoxide bis(acetylacetonate) in ethanol (1:39, v/v).

The solution for the mesoporous layer was prepared using 18NRT TiO_2 paste diluted in ethanol (1:3.5, w/w) and left under continuous rotation the day before. Mesoporous TiO_2 layer was deposited by spin coating at 6000rpm 40s. After drying at 80ºC 10min in a hot plate, it was heated following a heating plan shown in Figure 2.5.

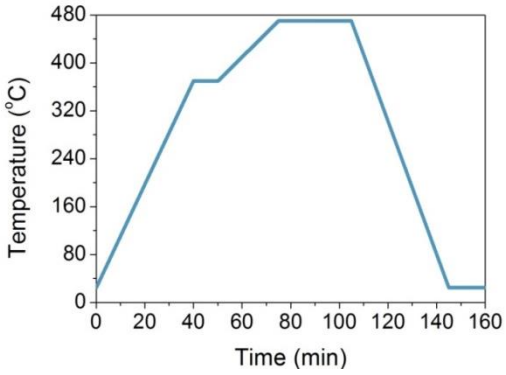

Figure 2.5 Heating plan.

The solutions of the different fullerene derivatives were prepared in anhydrous chlorobenzene (2mg/mL). The solutions were sonicated for 30 minutes and filtered with a 0.2µm PTFE filter. The self-assembled monolayers of fullerene derivatives were deposited by dip coating. The substrates were heated 10 minutes at 120ºC and immersed in these solutions for 24 hours. After this time, they were rinsed with anhydrous chlorobenzene and dried for 10 minutes at 120ºC.

The perovskite layer was prepared using methylammonium iodide and lead chloride as precursors. To prepare the solution, the precursors were mixed inside a glove box at a 3:1 mol ratio in DMF, respectively. The substrates were heated 10 minutes at 60ºC before the deposition. The solution was spin-coated at 500rpm for 5s and 2000rpm for 60s in air conditions. After the deposition, the substrates were heated at 100ºC during 90min in an oven under air stream.

The spiro-OMeTAD solution was prepared by dissolving 72.3mg of spiro-OMeTAD in chlorobenzene and adding 28.8μL of TBP and 17.5μL of a stock solution of 520mg/mL of Li-TFSI in acetonitrile. Spiro-OMeTAD was deposited by spin coating at 4000rpm for 30s with ramp of 5s. The gold deposition was performed by thermal evaporation at 10^{-6}mbar using an electron beam evaporation vacuum metallizer machine UNIVEX 250.

Chapter 3. Results and discussion

3.1. Current-Voltage curves

The J-V curves in forward and reverse scan of the different devices are shown in Figure 3.1-3.5. In Figure 3.1-3.3, the curves expose the effect of modifying the electron selective contact surface with a self-assembled monolayer of the different fullerenes, AM90 (TiO_2 CL/AM90), AM87 (TiO_2 CL/AM87) and IG321 (TiO_2 CL/IG321), respectively.

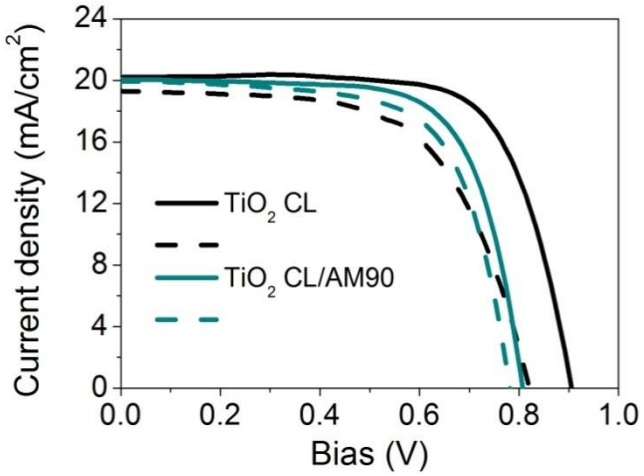

Figure 3.1 J-V curves showing the effect of the SAM of AM90, in forward (dashed lines) and reverse (solid lines) scan.

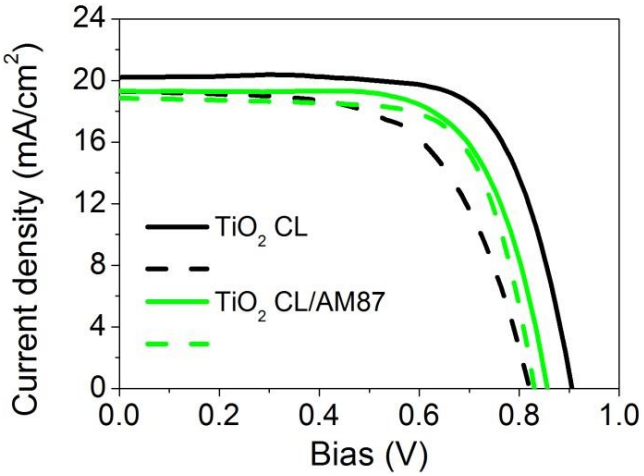

Figure 3.2 J-V curves showing the effect of the SAM of AM87, in forward (dashed lines) and reverse (solid lines) scan.

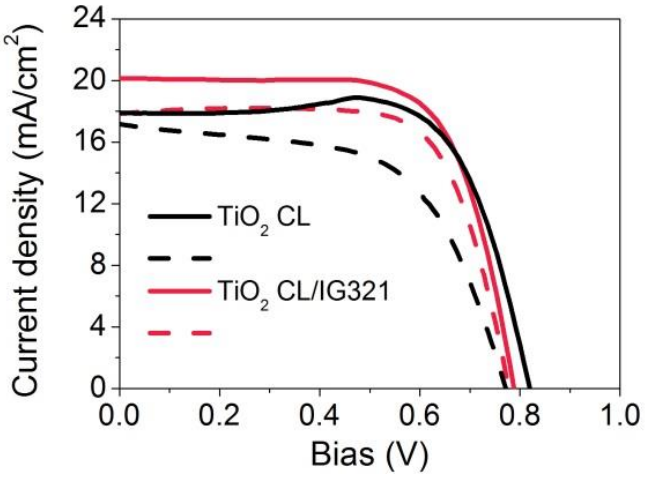

Figure 3.3 J-V curves showing the effect of the SAM of IG321, in forward (dashed lines) and reverse (solid lines) scan.

One highlighted effect is the reduction of the hysteresis, as shown in the hysteric index (HI) values in Table 3.1. The HI was calculated for the J-V curves shown in the figures with the following formula:[5]

$$HI = \frac{J_r\,(V_{oc}/2) - J_f\,(V_{oc}/2)}{J_r\,(V_{oc}/2)} \qquad \textbf{(3)}$$

Where $J_r(V_{oc}/2)$ is the current at $V_{oc}/2$ potential in the reverse scan direction and $J_f(V_{oc}/2)$ is the current at $V_{oc}/2$ potential in the forward scan direction. HI is zero for a sample with no hysteresis.

However, there is another important effect observed in these devices, which is the increase of the photocurrent when the SAM of IG321 is present. In the case of the other two fullerenes, the current density is similar to the reference (TiO_2 CL). The different behaviour of the three fullerenes could be explained by the change in the structure. AM87 and AM90 have different anchoring group but the contact surface with the perovskite is the same. Functionalizing the opposite part of the fullerene, the contact surface changes and it seems to improve the electron injection. CN groups in IG321 facing perovskite interface could help in coupling with $CH_3NH_3PbI_3$ perovskite. It has been observed that the presence of an amino group assists the formation of larger perovskite crystals.[30]

Figure 3.4 shows the effect of the SAM of IG321 in solar cells without CL (TiO_2/IG321). The current density presents a high increase; however, the reduction of the hysteresis is not as important as before. This could be attributed to a possible contact between the perovskite and the FTO surface.[6]

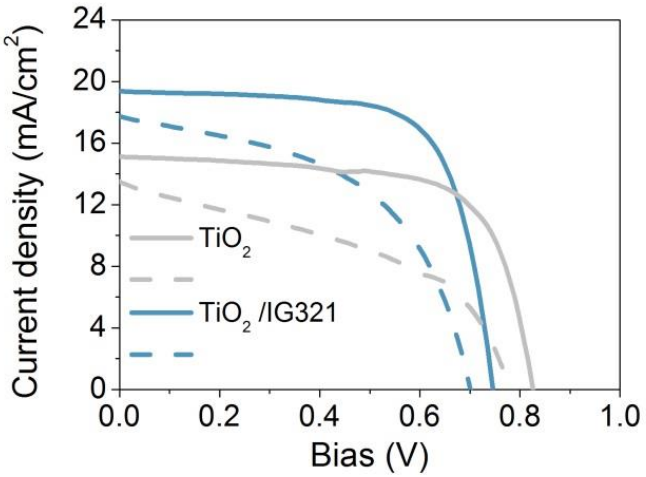

Figure 3.4 J-V curves showing the effect of the SAM of IG321 in solar cells without CL, in forward (dashed lines) and reverse (solid lines) scan.

Figure 3.5 shows the effect of removing the CL of the solar cells, both in the references and in the ones with a SAM of IG321. Although the photocurrent decreases when removing this layer, the reduction of photocurrent when SAM IG321 is used is significantly lower.

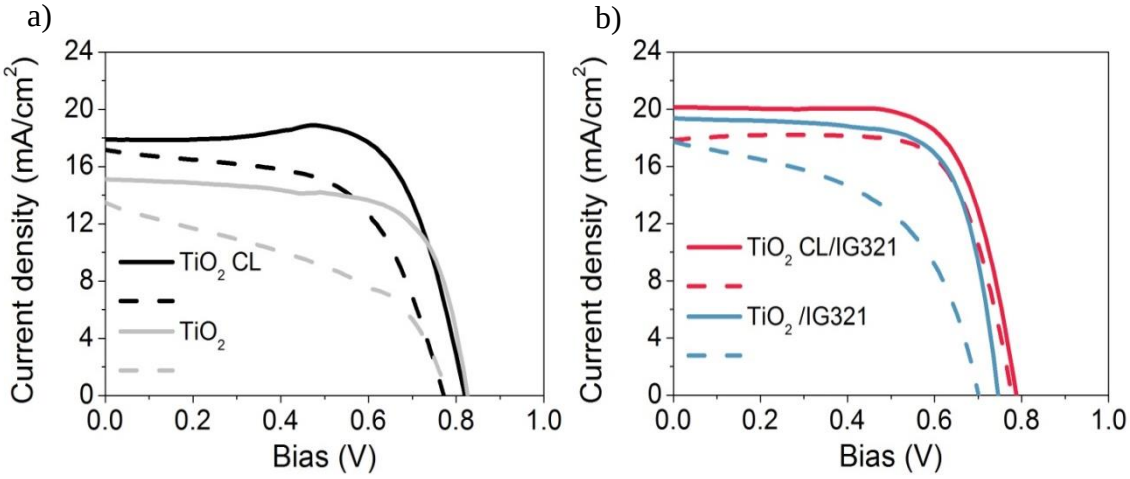

Figure 3.5 (a) J-V curves showing the effect of removing the CL in the references in forward (dashed lines) and reverse (solid lines) scan. **(b)** J-V curves showing the effect of removing the CL in the solar cells with a SAM of IG321 (solid line), in forward (dashed lines) and reverse (solid lines) scan.

Table 3.1 Characteristic parameters of the different devices. The averages were obtained using 20 samples of each type**.**

Device	Scan direction	J_{sc} (mA/cm^2)	V_{oc} (mV)	FF (%)	Eff (%)	HI
TiO_2 CL	reverse	19.8±0.6	909±15	75.4±2.1	13.5±0.6	0.081
	forward	19.3±0.6	827±18	63.4±2.2	10.1±0.7	
TiO_2 CL/AM90	reverse	19.2±0.5	822±13	71.4±1.9	11.2±0.3	0.023
	forward	18.7±0.8	797±15	70.3±2.0	10.47±0.22	
TiO_2 CL/AM87	reverse	19.2±0.6	839±12	67±4	10.9±0.8	0.041
	forward	18.7±0.5	818±8	66±5	10.0±0.8	
Device	**Scan direction**	**J_{sc}(mA/cm^2)**	**V_{oc} (mV)**	**FF (%)**	**Eff (%)**	**HI**
TiO_2 CL	reverse	17.1±1.3	792±18	68±5	9.1±0.9	0.143
	forward	14.5±2.2	728±54	49±9	5.4±1.7	
TiO_2	reverse	11.9±.1.7	817±16	64±5	6.2±1.0	0.303
	forward	11.2±1.8	768±35	41±3	3.6±0.7	
TiO_2 CL/IG321	reverse	18.1±1.3	780±11	63±13	8.9±1.9	0.013
	forward	16.6±0.9	779±6	71.4±2.1	9.2±0.5	
TiO_2/IG321	reverse	17.4±1.9	753±17	64±6	8.4±1.6	0.198
	forward	14±3	708±61	43±6	4.4±1.3	

3.2. Photoluminescence (PL)

PL spectra using an excitation wavelength of 650nm were measured. Figure 3.6a shows the PL spectra of the reference samples, samples with SAM of AM90 and samples with SAM of AM87, all with CL. In the inset, a zoom of the PL spectra of the samples modified with AM90 and AM87 is shown. In Figure 3.6b, the PL spectra at 650nm of reference samples with and without CL and samples with SAM of IG321with and without CL are shown.

The PL peak is quenched in samples with the SAM of the different molecules. The same effect but less important was obtained in the references without CL. The PL quenching observed in samples with SAM of fullerenes could be attributed to a good electronic coupling between the conduction band of perovskite and the LUMO of the different fullerenes.[8]

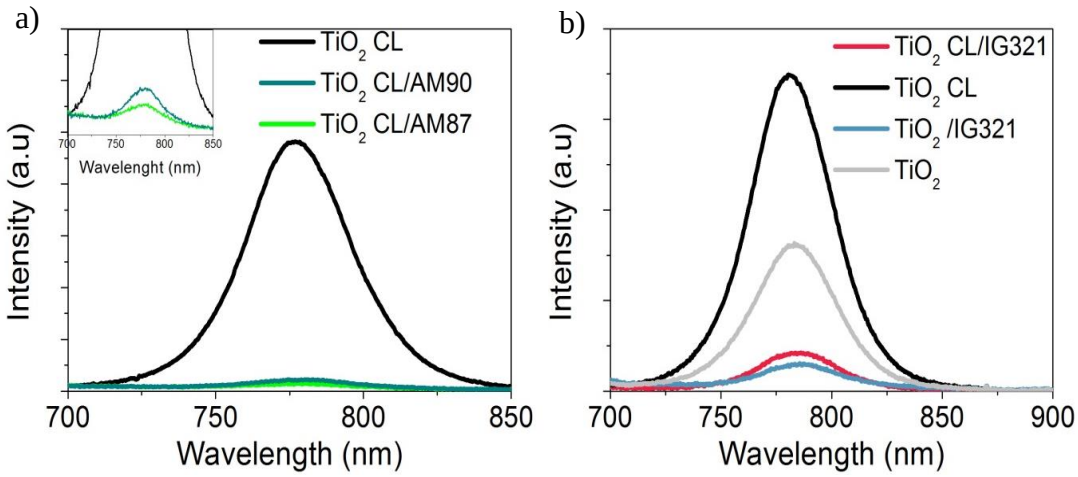

Figure 3.6 PL spectra, excitation wavelength 650nm, **(a)** for the reference samples and the ones with a SAM of AM90 and AM87, **(b)** for the reference samples and the ones with a SAM of IG321, with and without CL.

3.3. Electroluminescence (EL)

Electroluminescence and emission EQE measurements were performed at different voltages (1-3V). In Figure 3.7, the EL intensities of the different devices are shown at the different bias. Figure 3.8 shows the generated charge of the different devices at the different applied bias. Figure 3.9 shows the EQE of the different devices at the different bias.

In the EL intensities of the devices with CL, there is a decrease when there is a SAM of AM90 or AM87, see Figure 3.7a. However, in Figure 3.7b, a slight increase is observed with the SAM of IG321. When the CL is removed, a high increase in the intensity of the reference devices is obtained, but the increase observed when the CL is present with IG321 is not observed, being the intensity of the same order with and without the CL.

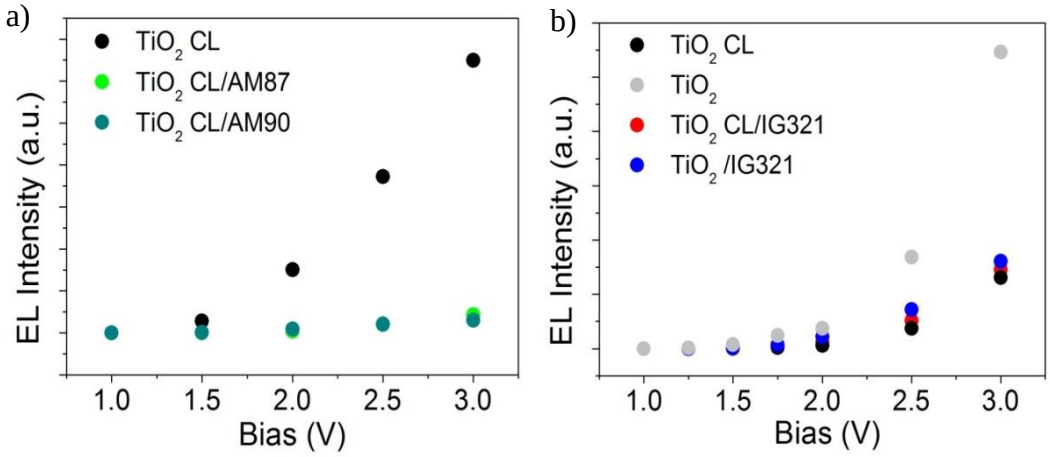

Figure 3.7 (a) EL intensity at different bias of the references and the devices with a SAM of AM87 and AM90. **(b)** EL intensity at different bias of the references and the devices with a SAM of IG321 with and without CL.

The generated charge by devices is obtained from the chronoamperometry. The charge of the devices with a SAM of AM90 and AM87 show a slight decrease, however, in the devices with IG321 increases. When removing the compact layer, there is an even higher increase in the injected charge. The charge obtained by modifying the surface with IG321 in the devices without CL is similar to the reference without CL. Note that the fullerene also has an important role on the control of injected charge at an applied bias. AM90 and AM87 reduce the charge respect the reference sample while opposite behaviour is observed when IG321 is used.

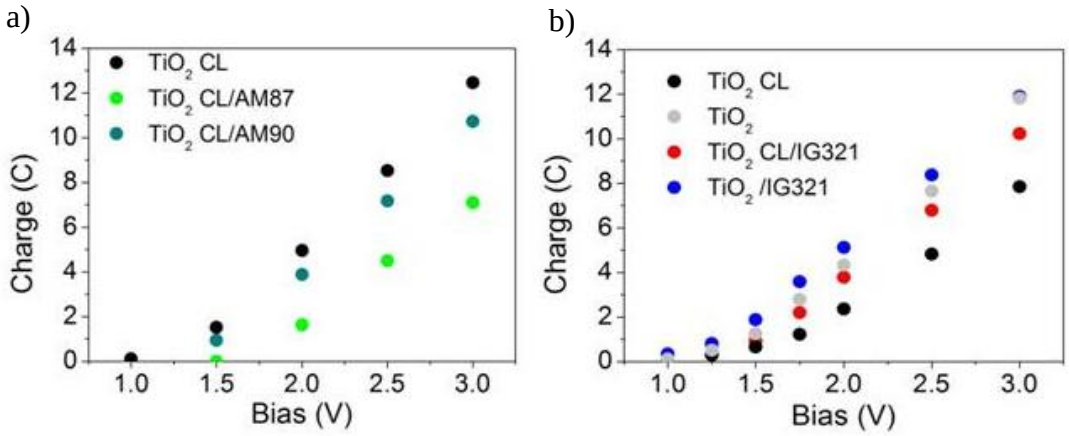

Figure 3.8 (a) Generated charge at different bias of the references and the devices with a SAM of AM87 and AM90. **(b)** Generated charge at different bias of the references and the devices with a SAM of IG321 with and without CL.

The emission EQE can be obtained with the following expression:[34]

$$EQE(\%) = \frac{number\ of\ emitted\ photons}{number\ of\ injected\ electrons} \quad \textbf{(4)}$$

The number of electrons is obtained from the generated charge. The number of photons is obtained from the EL intensity compared with a commercial LED whose EQE is known. When comparing the EQE of the devices with AM90 and AM87 with the reference, the EQE of the references are an order of magnitude higher than the others. This is due to the lower charge and the lower emission when the SAM of these fullerene derivatives is present. In the comparison of the devices with IG321 with the reference, with and without CL, the EQE of the references without CL are an order of magnitude higher than the others. Interestingly, devices without TiO_2 CL presents higher emission than their corresponding reference samples with CL. This fact can be atributed to a lower non-radiative recombination as also points out the higher V_{oc} obtained for samples without CL in comparison with samples with CL, see Table 3.1.

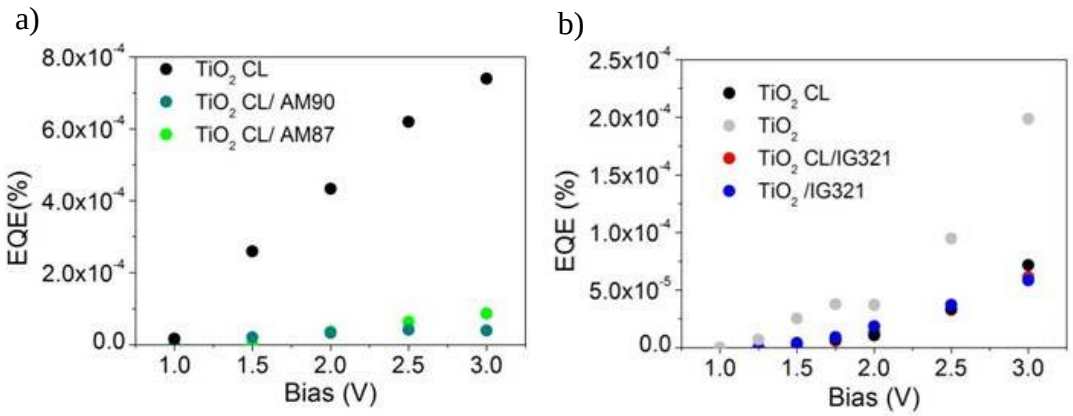

Figure 3.9 (a) EQE at different bias of the references and the devices with a SAM of AM87 and AM90. **(b)** EQE at different bias of the references and the devices with a SAM of IG321 with and without CL.

3.4. Scanning Electron Microscopy (SEM)

The structure of the cells has been analyzed by Scanning Electron Microscopy. In Figure 3.10, a SEM image shows the layer of FTO, the CL of TiO_2, the mesoporous TiO_2 and the perovskite layer, though the CL layer is not visible enough. The approximate thickness of these layers was measured in the SEM, giving the values shown in Table 3.2. The perovskite pierces the mesoporous layer, so that the value shown in Table 3.2 is the overlayer.

Table 3.2 Approximate values of the thickness of the layers shown in the SEM image.

Layer	Thickness(nm)
FTO	400
TiO_2 CL	40
TiO_2 NS	100
Perovskite	400

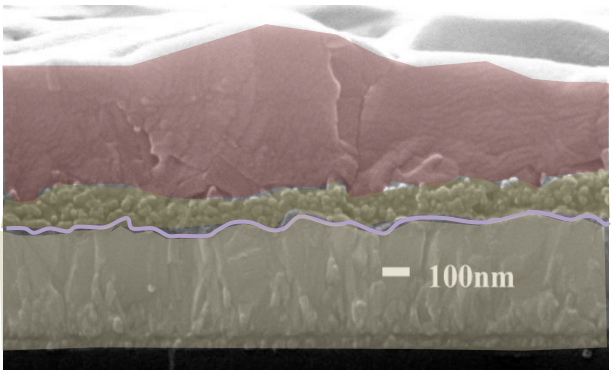

Figure 3.10 SEM image showing the FTO (grey), CL TiO_2 (purple), NS TiO_2 (green) and perovskite layer (red).

Chapter 4. Conclusion

Different PSCs have been prepared and characterized. To improve the efficiency of the SCs, the TiO_2 surface was modified with a SAM of different fullerene derivatives due to the fact that the conjugated system forming the structure of the fullerenes is supposed to improve the electron extraction into the ESC. Fullerene derivative IG321 has demonstrated to enhance the electron injection; moreover, it has reduced the hysteresis of the J-V curves usually present in PSCs. Fullerene derivatives AM87 and AM90 have not enhanced significantly the current density, however, they have a strong effect on the hysteresis reduction. Furthermore, some devices without compact layer were prepared and characterized. With no compact layer, the hysteresis reduction is not as important; however, the use of IG321 SAM rectifies the photocurrent reduction observed when compact layer is removed.

The PL and EL were also measured and the EQE of the different devices were calculated and compared at the different applied bias. The effect of the SAM of fullerene derivatives in the PL measurement resulted in a PL quenching, decreasing the emission intensity. In the case of the EL and the EQE, the same effect was observed. Removing the compact layer decreased the PL, however, the EL emission was highly enhanced and consequently the EQE. The type of fullerene used plays an important role in the charge injection, increasing or decreasing the charge observed for a fixed applied voltage with respect to the reference sample without SAM. Further research will be needed in order to stablish the physical origin of these references.

Chapter 5. Future work and perspectives

Taking into account the results obtained in this work, there are several future works that can be carried out. First of all, more fullerene derivatives could be employed to functionalize the TiO_2 surface in order to find the appropriate anchoring group and the part in contact with the perovskite, as it has an important effect on the crystallization of the perovskite and the electron extraction.

Another interesting future work could be to replace the n-type contact of the SC. It has been reported that efficient devices could be obtained with this configuration.[6] Furthermore, the fullerene derivatives could be embedded inside the perovskite to improve its properties.

References

(1) Gao, P.; Gratzel, M.; Nazeeruddin, M. K. *Energy & Environmental Science* **2014**, *7*, 2448.

(2) Jung, H. S.; Park, N. G. *Small* **2015**, *11*, 10.

(3) Park, N.-G. *Materials Today* **2015**, *18*, 65.

(4) Heo, J. H.; Im, S. H.; Noh, J. H.; Mandal, T. N.; Lim, C.-S.; Chang, J. A.; Lee, Y. H.; Kim, H.-j.; Sarkar, A.; NazeeruddinMd, K.; Gratzel, M.; Seok, S. I. *Nat Photon* **2013**, *7*, 486.

(5) Sanchez, R. S.; Gonzalez-Pedro, V.; Lee, J.-W.; Park, N.-G.; Kang, Y. S.; Mora-Sero, I.; Bisquert, J. *The Journal of Physical Chemistry Letters* **2014**, *5*, 2357.

(6) Wojciechowski, K.; Leijtens, T.; Siprova, S.; Schlueter, C.; Hörantner, M. T.; Wang, J. T.-W.; Li, C.-Z.; Jen, A. K. Y.; Lee, T.-L.; Snaith, H. J. *The Journal of Physical Chemistry Letters* **2015**, *6*, 2399.

(7) Wojciechowski, K.; Stranks, S. D.; Abate, A.; Sadoughi, G.; Sadhanala, A.; Kopidakis, N.; Rumbles, G.; Li, C.-Z.; Friend, R. H.; Jen, A. K. Y.; Snaith, H. J. *ACS Nano* **2014**, *8*, 12701.

(8) Li, Y.; Zhao, Y.; Chen, Q.; Yang, Y. M.; Liu, Y.; Hong, Z.; Liu, Z.; Hsieh, Y. T.; Meng, L.; Yang, Y. *Journal of the American Chemical Society* **2015**, *137*, 15540.

(9) Green, M. A. *Energy Policy* **2000**, *28*, 989.

(10) Smestad, G. P. *Optoelectronics of Solar Cells*; Society of Photo Optical, 2002.

(11) Fahrenbruch, A.; Bube, R. *Fundamentals Of Solar Cells: Photovoltaic Solar Energy Conversion*; Elsevier Science, 2012.

(12) Bisquert, J.; Cahen, D.; Hodes, G.; Ruhle, S.; Zaban, A. *Journal of Physical Chemistry B* **2004**, *108*, 8106.

(13) Sun, S. S.; Dalton, L. R. *Introduction to Organic Electronic and Optoelectronic Materials and Devices*; CRC Press, 2008.

(14) Bisquert, J.; Cahen, D.; Hodes, G.; Rühle, S.; Zaban, A. *The Journal of Physical Chemistry B* **2004**, *108*, 8106.

(15) Fabregat-Santiago, F.; Garcia-Belmonte, G.; Mora-Sero, I.; Bisquert, J. *Physical Chemistry Chemical Physics* **2011**, *13*, 9083.

(16) Razykov, T. M.; Ferekides, C. S.; Morel, D.; Stefanakos, E.; Ullal, H. S.; Upadhyaya, H. M. *Solar Energy* **2011**, *85*, 1580.

(17) Goetzberger, A.; Hebling, C. *Solar Energy Materials and Solar Cells* **2000**, *62*, 1.

(18) Chapin, D. M.; Fuller, C. S.; Pearson, G. L. *Journal of Applied Physics* **1954**, *25*, 676.

(19) Green, M. A. *Physica E: Low-dimensional Systems and Nanostructures* **2002**, *14*, 11.

(20) Weinberger, B. R.; Akhtar, M.; Gau, S. C. *Synthetic Metals* **1982**, *4*, 187.

(21) Tang, C. W. *Applied Physics Letters* **1986**, *48*, 183.

(22) Hagfeldt, A.; Boschloo, G.; Sun, L.; Kloo, L.; Pettersson, H. *Chemical*

Reviews **2010**, *110*, 6595.

(23) Grätzel, M. *Inorganic Chemistry* **2005**, *44*, 6841.

(24) Kojima, A.; Teshima, K.; Shirai, Y.; Miyasaka, T. *Journal of the American Chemical Society* **2009**, *131*, 6050.

(25) Snaith, H. J. *The Journal of Physical Chemistry Letters* **2013**, *4*, 3623.

(26) Leguy, A. M. A.; Frost, J. M.; McMahon, A. P.; Sakai, V. G.; Kockelmann, W.; Law, C.; Li, X.; Foglia, F.; Walsh, A.; O/'Regan, B. C.; Nelson, J.; Cabral, J. T.; Barnes, P. R. F. *Nat Commun* **2015**, *6*.

(27) Sum, T. C.; Mathews, N. *Energy & Environmental Science* **2014**, *7*, 2518.

(28) Leijtens, T.; Eperon, G. E.; Pathak, S.; Abate, A.; Lee, M. M.; Snaith, H. J. *Nat Commun* **2013**, *4*.

(29) Völker, S. F.; Collavini, S.; Delgado, J. L. *ChemSusChem* **2015**, *8*, 3012.

(30) Li, B.; Chen, Y.; Liang, Z.; Gao, D.; Huang, W. *RSC Advances* **2015**, *5*, 94290.

(31) Perednis, D.; Gauckler, L. J. *Journal of Electroceramics* **2005**, *14*, 103.

(32) Krebs, F. C. *Solar Energy Materials and Solar Cells* **2009**, *93*, 394.

(33) Mattox, D. M. *The Foundations of Vacuum Coating Technology*; Noyes Publications/William Andrew Pub., 2004.

(34) Hassan, A. M.; Chemistry, U. o. S. C. *Theoretical, Experimental, Device Fabrication, and Degradation Studies of Materials for Optoelectronic Devices*; University of Southern California, 2007.

Annex

Synthesis of the fullerene derivatives

For the synthesis of AM90 fullerene, a mixture of 4-Carboxybenzaldehyde (104 mg, 0.70 mmol), C_{60} (100 mg, 0.14 mmol) and sarcosine (25 mg, 0.28 mmol) were dissolved in toluene and the mixture was refluxed for 5 hours. The reaction mixture was allowed to reach room temperature and the solvent was removed under vacuum. The crude was purified by flash column chromatography on SiO_2, using CS2/Toluene and then Toluene/ethyl acetate (2:1). The black solid obtained was further purified by repeated (3x) precipitation and centrifugation in methanol to yield the corresponding hybrids as black solids. ^{1}H NMR (DMSO-d_6, 300 MHz, 298 K) δ 13.0 (s, 1H), 8.04 (d, *J* = 7.6 Hz, 2H), 7.94 (d, *J* = 7.8 Hz, 2H), 5.22 (s, 1H), 5.11 (d, *J* = 9.4, 1H), 4.35 (d, *J* = 9.4 Hz, 1H), 3.17 (s, 3H).

For synthesizing AM87 fullerene, in a dried 500 mL round bottom flask, 358 mg (0.497 mmol) of C_{60} was dissolved in 250 mL of dry toluene and sonicated for 15 min. 3,4-Bis(bromomethyl)benzoic acid (156.2 mg 0.507 mmol), potassium iodide (585 mg 3.5 mmol), and 18-Crown-6 (250 mg 0.94 mmol) were sequentially added while stirring under dry nitrogen. The reaction mixture was stirred and heated at reflux for 14 hours. The reaction mixture was allowed to reach room temperature and the solvent was removed under vacuum. The crude was purified by flash column chromatography on SiO_2 using (CS_2/Toluene and then Toluene/THF (2:1)). The black solid obtained was further purified by repeated (3x) precipitation and centrifugation in methanol to yield the corresponding hybrid as black solid. ^{1}H NMR (DMSO-d_6, 300 MHz, 298 K) δ 13.1 (s, 1H), 8.35 (d, *J* = 1.6 Hz, 1H), 8.14 (dd, *J* = 7.8 Hz, *J* = 1.6 Hz, 1H), 7.90 (d, *J* = 7.8 Hz, 1H), 5.06 (m , 2H), 4.66 (m , 2H).

For synthesizing IG321 fullerene, a mixture of 4-Carboxybenzaldehyde (14.2 mg, 0.09 mmol), C_{60}-CN_2 (80 mg, 0.10 mmol) and sarcosine (41.4 mg, 0.47 mmol) were dissolved in chlorobenzene (20 mL) and the mixture was refluxed for 20 hours. The reaction mixture was allowed to reach room temperature and the solvent was removed under vacuum. The crude was purified by flash column chromatography on SiO_2, using CS2/Toluene and then Toluene/THF (2:1). The black solid obtained was further purified by repeated (3x) precipitation and centrifugation in methanol to yield the corresponding hybrids as black solids. ^{1}H NMR (DMSO-d_6, 300 MHz, 298 K) δ 13.0 (s, 1H), 8.25-7.59 (m), 5.02-4.56 (m), 2.90-2.60 (m); MS-ESI m/z 950.1 $[M+H]^+$.

Characterization of the fullerene derivatives

The different fullerenes were characterized by measuring the absorbance spectra and cyclic voltammetries, as shown in Figure 1 and Figure 2. From these measurements, some characteristic parameters are obtained, as shown in Table 1 and Table 2.

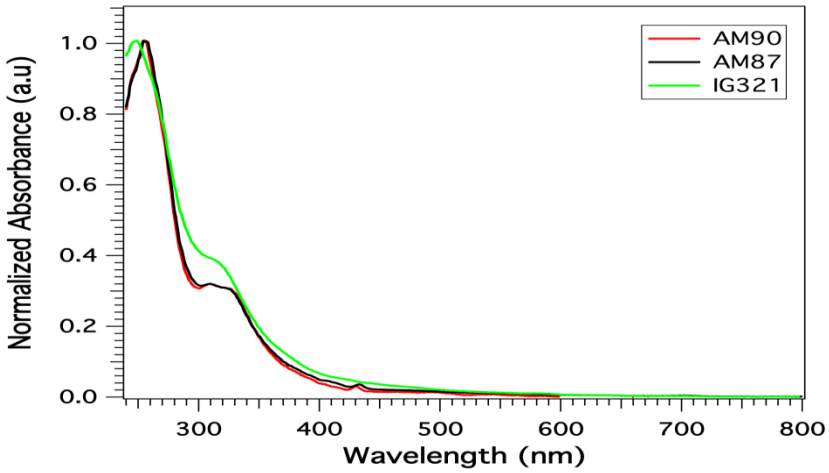

Figure 1. Normalized Absorbance spectra of the fullerene derivatives IG321 (green curve), AM87 (black curve) and AM90 (red curve).

The AM87 and AM90 absorbance spectra are pretty similar, but the wavelength of the maximum absorbance is slightly lower in the case of IG321. The optical bandgaps do not vary significantly, being a bit lower in AM87. As shown in Table 1, the HOMO energy is around -5.95eV for AM87, -6eV for AM90 and -6.2eV for IG321.

Table 1. Wavelength of the maximum absorption, optical gap and HOMO energy of the different fullerenes extracted from the absorbance spectra.

Compound	λ_{max}(nm)	$E_{gap,opt}$(eV)	E_{HOMO} (eV)
AM90	256	2	-6
AM87	256	1.95	-5.95
IG321	250	2	-6.2

From CV measurements, Figure 2, the different reduction potentials and the LUMO energy could be obtained; their values are presented in Table 2. As shown in other parameters, AM87 and AM90 have a similar behavior but IG321 differs in some of them. The LUMO has lower energy than in the other two compounds, which could have an effect on the charge extraction.

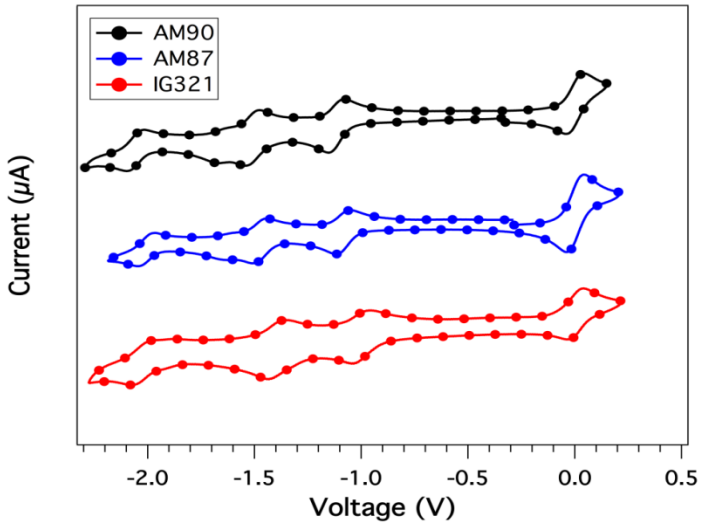

Figure 2. Cyclic voltammetry measurements for IG321 (red curve), AM87 (blue curve) and AM90 (black curve).

Table 2. Reduction potentials and LUMO Energy of the different fullerenes extracted from the CV measurements.

Compound	E^1_{red} (eV)	E^2_{red}(eV)	E^3_{red}(eV)	E^4_{red}(eV)	E_{LUMO} (eV)
AM90	-1.11	-1.51	-1.67	-2.05	-4.06
AM87	-1.08	-1.47	-1.62	-1.99	-4.00
IG321	-0.99	-1.39	-2.01	-	-4.20